Research Article

Xingqiang Xiong, Changrong Li*, and Lu Chen

Modification of Al_2O_3 inclusions in SWRH82B steel by La/Y rare-earth element treatment

https://doi.org/10.1515/htmp-2022-0032
received October 28, 2021; accepted March 27, 2022

Abstract: The experimental schemes of lanthanum (La) treatment, yttrium (Y) treatment, and La/Y mixed treatment of inclusions in SWRH82B steel were used. The size distribution, number density, inter-surface distance, the degree of homogeneity, and the area density of inclusions in the test steel were determined. The results show that the rare earths have a certain refinement and homogenization effect on the inclusions, and the mixed rare earths have the best effect on the inclusions in the steel. The average size of inclusions after mixed rare-earth treatment is 1.23 μm, the average size of inclusions after rare-earth La treatment is 1.79 μm, and the average size of inclusions after rare-earth Y treatment is 1.37 μm. Thermodynamic calculations show that the affinity of rare earths to oxygen in steel is higher, and the affinity to sulfur is lower. La and oxygen–sulfur have a higher affinity, and the affinity of Y and oxygen–sulfur is lower. In addition to single inclusions, there are complex inclusions in the steel.

Keywords: rare earth, mixed treatment, SWRH82B, inclusions

1 Introduction

The finished products of SWRH82B wire rod steel are used in railways, highway bridges, crane beams, nuclear reactors, long-span bridges "cable rods," and the construction of prestressed concrete water pipelines [1]. The drawing performance of 82B wire rod steel affects the performance of the product. When developing high-quality hard wires, we have been pursuing high wire processing performance to prevent breakage during the drawing process. The nonmetallic inclusions in the hard wire steel have an important influence on the wire breakage during the cold drawing process, which will cause the steel to break early in the actual application. The number, size, type, and distribution of the inclusions are very important to the performance of the hard wire steel [2–5]. The production practice of metal product enterprises has proved that inclusions are easy to cause a brittle fracture in the steel drawing process.

Zejin studied the reasons for the brittle fracture of SWRH82B wire rod steel, and the results show that it is caused by Al_2O_3, CaO, and SiO_2 inclusions. The method of refinement of inclusions is used to improve the properties of steel [6]. Zhao et al. studied the microstructure, fracture morphology, composition, and distribution of SWRH82B wire rod steel to find the causes of internal defects [7]. The results show that there are serious segregation, uneven microstructure, and uneven distribution of inclusions in the steel [7]. Hao et al. studied the influence of calcium treatment on inclusions in H13 die steel, calculated the transformation process of inclusions in steel by thermodynamics, and discussed the influence of calcium treatment on the composition and structure of inclusions, but it only uses a separate Ca treatment [8]. Zheng et al. studied different Ti/Mg ratios to treat inclusions in steel and studied the effects of inclusion characteristics, sulfur content, and deoxidation product quantity on the precipitation behavior of MnS [9]. The results showed that mixed addition is better than Ti treatment alone or Mg treatment alone. Therefore, it can be considered to use mixed rare earth to treat the inclusions in steel [9].

* **Corresponding author: Changrong Li,** School of Materials and Metallurgy, Guizhou University, Guiyang 550025, China; Guizhou Key Laboratory of Metallurgical Engineering and Process Energy Conservation, Guiyang 550025, China, e-mail: crli@gzu.edu.cn
Xingqiang Xiong: School of Materials and Metallurgy, Guizhou University, Guiyang 550025, China; Guizhou Key Laboratory of Metallurgical Engineering and Process Energy Conservation, Guiyang 550025, China, e-mail: xxq20141101@163.com
Lu Chen: School of Materials and Metallurgy, Guizhou University, Guiyang 550025, China; Guizhou Key Laboratory of Metallurgical Engineering and Process Energy Conservation, Guiyang 550025, China, e-mail: chen841283779@163.com

Yue et al. studied the type, morphology, and distribution of non-metallic inclusions in weathering steel by adding rare earths. The results showed that rare earths changed the types and morphologies of inclusions in weathering steel. Small spherical rare earth oxysulfides and rare earth sulfides replace the elongated MnS inclusions in the steel. Rare earth inclusions are evenly distributed, and most of the inclusions are less than 2 μm in size [10]. Huang et al. studied the modification process of rare earth Ce on magnesium–aluminum spinel and graphite in steel [11]. The results show that the rare earth Ce has a good modification effect on Al_2O_3 and $MgAl_2O_4$, has refined the inclusions in the steel, improved the fatigue resistance of the steel, and prolonged the service life. [11]. There are many studies on thermodynamics [12–17] and kinetics [18–20] of a single element (calcium–magnesium treatment or rare-earth treatment) in the treatment of inclusions in steel and less research on the treatment of inclusions in steel with mixed rare earths.

In this study, two kinds of rare earth elements (lanthanum [La] and yttrium [Y]) were added to SWRH82B steel, and the influence of rare earth on the number, size, inter-surface distance, degree of homogeneity, and area density of inclusions in the steel was analyzed. Therefore, the modification effects of different treatment methods were compared. In addition, thermodynamic calculations were used to analyze the formation sequence of rare-earth inclusions and the types of inclusions that may exist in molten steel.

2 Experiment

This experiment used pure iron, recarburizer, Fe–Mn alloy, aluminum bar, rare earths La and Y as raw materials and is smelted in an intermediate frequency induction furnace.

Table 1: Chemical composition of SWRH82B (wt%)

Element	C	Si	Mn	P	S
Content	0.79–0.86	0.15–0.35	0.6–0.9	≤0.03	≤0.03

The element content is referenced to SWRH82B steel, and its chemical composition is shown in Table 1.

Experimental procedure is as follows: 10 kg of pure iron, recarburizer, and Fe–Mn alloy were added into a crucible with a capacity of 20 kg; when the medium-frequency induction furnace was heated to 1,873 K, the molten steel was stirred to melt completely. Stirring method is as follows: an aeration device was connected to the top of the induction furnace; when the experimental raw materials and rare earths were added, the aeration device was passed through a high-temperature aeration pipe and argon gas was introduced from the top to the bottom to stir the molten steel to realize the uniformity of the raw materials. After 5 min, an aluminum bar was added to deoxidize and the molten steel was stirred. After 5 min, the rare earth was added and the molten steel was stirred. After holding for 3 min, the molten steel was poured into the mold to cool in the air, and the molten steel was sampled after solidification and cooling. The general flow of the test is shown in Figure 1.

The whole experiment was divided into three groups, and different rare earths were added under the same experimental conditions. 1# test steel added 0.01% rare earth La and 0.01% rare earth Y, 2# test steel added 0.02% rare earth La, and 3# test steel added 0.02% rare earth Y. The yield of rare earth is taken as 10% for calculation and addition [21]. However, the specific test steel composition is subject to the inductively coupled plasma (ICP) test results (ICP-OES: PerkinElmer 8300; PerkinElmer ICP 2100; ICAP7400; PerkinElmer Optima 5300 DV; OPTIMA 8000). ICP is the main light source for atomic emission spectroscopy and mass spectrometry; with ICP as the center, multiple detection units are installed around, forming a multi-element analysis system. Quantitative analysis of elements is performed by accepting emission spectra of different wavelengths, the atoms to be measured are in an excited state, and their respective characteristic spectral lines can be simultaneously emitted for element content determination. The average value was obtained by measuring three times, and the results are shown in Table 2.

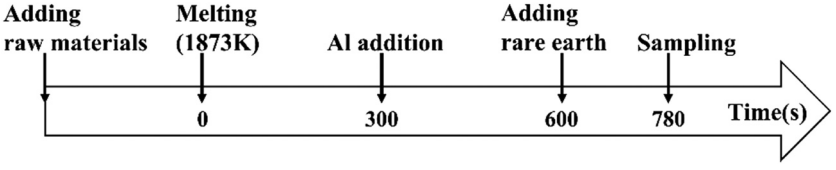

Figure 1: The general process of the test.

Table 2: Chemical composition of test steel (wt%)

Number	C	Mn	Si	P	S	Al	O	La	Y	Fe
1#	0.820	0.80	0.21	0.019	0.006	0.072	0.0057	0.012	0.013	bal.
2#	0.818	0.81	0.21	0.018	0.007	0.080	0.0082	0.023	—	bal.
3#	0.822	0.81	0.20	0.019	0.007	0.079	0.0096	—	0.024	bal.

The finished product of the experiment was cut into small samples, the size of the sample was 10 mm × 10 mm × 12 mm. The sample was treated with sandpaper (from 240 to 3,000 mesh), then polished (the model of the polishing paste is W2.5 and the finish range is 0.025–0.012 mm), and finally cleaned with ethanol and dried with a blower. Under the magnification of 1,000 times, energy-dispersive spectroscopy (EDS) and scanning electron microscope (SEM) instrument were used to photograph the sample and continuously photograph 100 SEM images. The captured SEM images were imported into Image-ProPlus software (Image-ProPlus 6.0; Media Cybernetics, Rockville, MD, USA) to analyze the size distribution, number density, inter-surface distance, degree of homogeneity, and area density of inclusions in the sample steel.

3 Experimental results

3.1 Morphology and composition of inclusions

To determine whether the rare earths La and Y have an effect on the inclusions, SEM and EDS were used to detect the inclusions in the test steel (the results are shown in Figures 2 and 3). Figure 2 is the morphology and composition distribution diagram of the inclusions, and Figure 3 is the EDS diagram of the corresponding inclusions. 1# in Figure 2 is the inclusion after adding rare earths La and Y, area (2) is the inclusion containing La, and area (a) and area (3) are the inclusions containing Y. It can be seen that the La-containing inclusions are wrapped by the Y-containing inclusions. At the same time, it shows that after the rare earths La and Y are added, La reacts first, followed by Y, and the La-containing inclusions serve as the nucleation core. Both rare earths have played a modifying role. 2# in Figure 2 is the inclusion after adding rare earth La. Area (1) is the La-containing inclusion, and area (2) is basically Al_2O_3 inclusion. According to the morphology of the inclusions, it can be seen that the La-containing inclusions half-wrapped the Al_2O_3 inclusions, and the rare earth La also has a modification effect. 3# in Figure 2 is the inclusion after adding rare earth Y. The entire area of the inclusion contains Y, Al, O, and S elements. It shows that after rare earth Y is added, the Al_2O_3 inclusions in the steel are modified. Combining the reaction effects of three inclusions, we can conclude that the addition of rare earths modifies the inclusions in the steel to varying degrees. The two-dimensional morphology of the inclusions tends to be round, and the size of the inclusions is also smaller.

It is not convincing to photograph a single inclusion. To confirm the modification effect of rare earth, 20 inclusions were detected by EDS and the average chemical composition of the inclusions in the sample steel was calculated. The results are shown in Figure 4. When adding rare earths La and Y, the average content of La is 33.4%, and the average content of Y is 20.5%; when

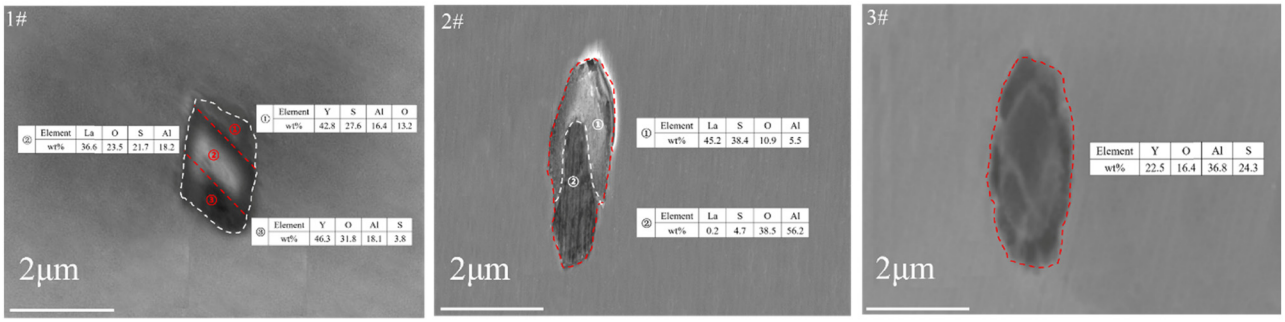

Figure 2: Composition distribution of inclusions in test steel.

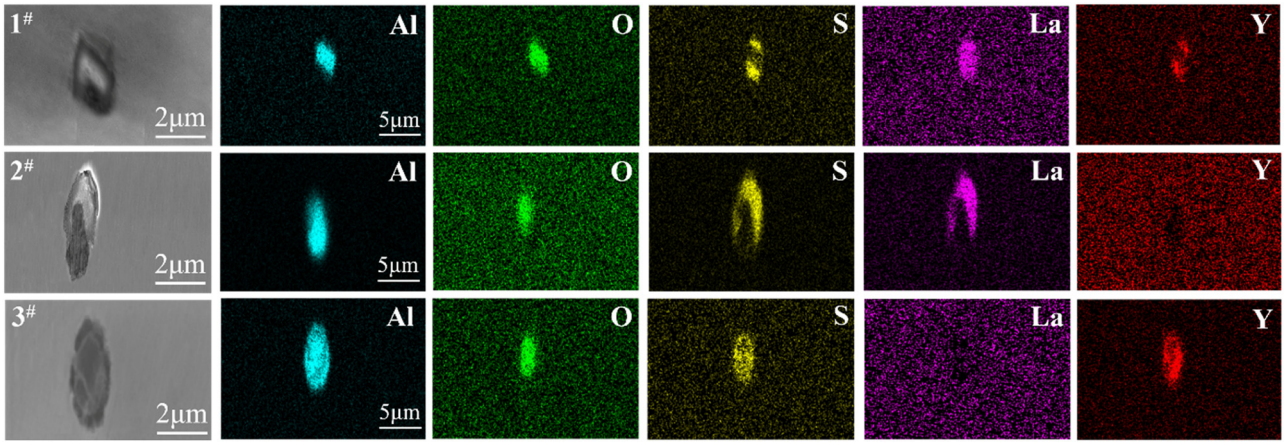

Figure 3: Sweep of inclusions in test steel.

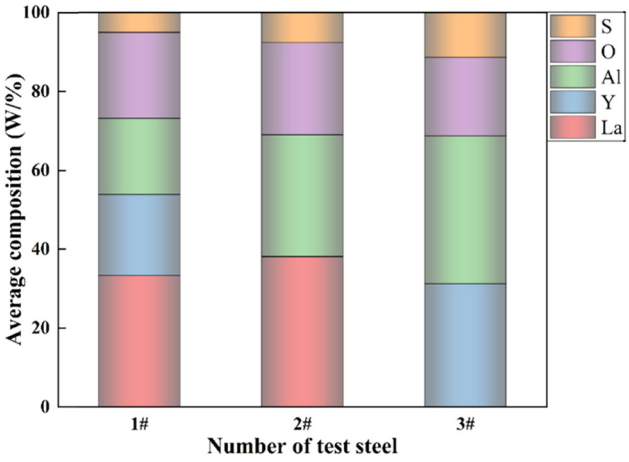

Figure 4: Chemical composition of inclusions in test steel.

adding rare earth La, the average content of La is 38.2%; when adding rare earth Y, the average content of Y is 31.1%. Because the total amount of inclusions added in the three test steels is the same. Combining the results in Figure 4, it is concluded that the amount of mixed rare earth added is the highest, followed by rare earth La, and rare earth Y is the lowest.

To further determine the distribution of elements, a ternary phase diagram was made for 20 EDS detection results, and the results are shown in Figure 5. Comparing the atomic compositions and proportions of the three test steels, it can be concluded that after adding rare earths La and Y, the distribution of inclusions in the steel is basically concentrated on La, Y, O, and S (1# in Figure 5). After adding rare earth La, the composition distribution of inclusions is mostly concentrated on La, O, and S (2# in Figure 5). After adding rare earth Y, the composition distribution of inclusions is mostly concentrated on Y, O, and S (3# in Figure 5). Moreover, the inclusions have the highest degree of element aggregation in the sample steel with mixed rare earths. Based on the above analysis, it is shown that after the addition of rare earths, the inclusions have been modified to varying degrees. Among them, the effect of adding mixed rare earth is the best, which may represent a higher use value.

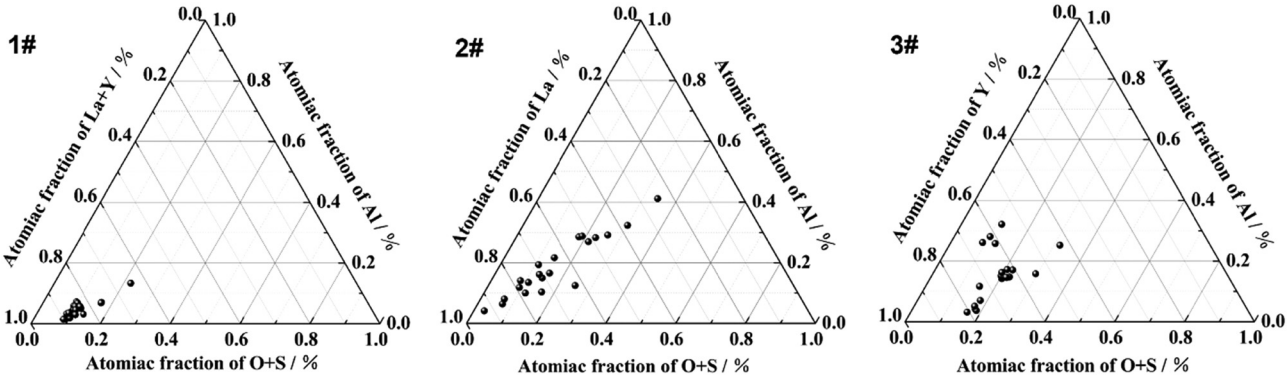

Figure 5: Elements' distribution of inclusions in test steel.

3.2 Characteristics of inclusions

Figure 6 is the variation curve of the number of inclusions on 1 μm^2 with the diameter of inclusions. The curve is similar to a normal distribution (the variable corresponding to the peak of the curve is the mean, and the mean refers to the independent variable of the centralized distribution). The variable (inclusion diameter) corresponding to the peak of the number density of inclusions in Figure 6 is about 1.4 μm, so the size of most of the inclusions is between 1 and 2 μm. The number densities of inclusions with diameters between 1 and 2 μm in the three test steels are very large, indicating that the number of inclusions with smaller diameters is larger and the refining effect is good. Because after adding rare earth, the inclusions in the steel will accumulate and cause the large-size inclusions to float up or react with the inclusions to refine the inclusions. When the number of large-size inclusions decreases and the number of small-size inclusions increases, it means that the refinement effect is better [22,23]. However, the number of inclusions in 1# steel with a diameter distribution between 1 and 2 μm is the largest, indicating that the mixed rare earth treatment effect is better.

The data of inclusions are obtained by Image-ProPlus software, the data are statistically integrated, and the minimum inter-surface distance is obtained (as shown in Figure 7). It can be seen from Figure 7 that the proportions of the minimum inter-surface distance of inclusions in 1#, 2#, and 3# steels greater than 10 μm are 74, 72, and 64%. When the diameter of the inclusions is less than 1 μm and the minimum inter-surface distance is greater than 10 μm, the influence of the inclusions on the properties of the steel can be ignored [24]. The proportion of inclusions in 3# steel whose inter-surface distance is greater than 10 μm is obviously smaller than that of 1# and 2# steels, meaning that compared with 3# steel, 1# and 2# steels have better treatment effects and 1# steel is the best.

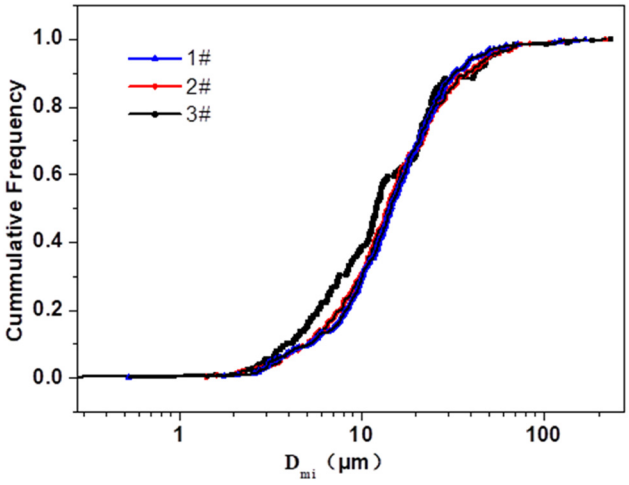

Figure 7: Minimum inter-surface distance distribution curve of inclusions in test steel.

The average size, degree of homogeneity (parameter of the distribution of inclusions, the larger the value, the more uniform the distribution of inclusions), and the number of inclusions in the three groups of test steels are obtained by statistics. The results are shown in Figure 8. The degree of homogeneity of inclusions in 1# test steel is the largest, 2# test steel is the second, and 3# test steel is the smallest. It shows that the distribution of inclusions in 1# test steel is the most even, the effect of 2# test steel is the second, and 3# test steel is the worst. Meanwhile, the average size of inclusions in 1# test steel is the smallest, while that in 2# test steel is the largest. Combined with

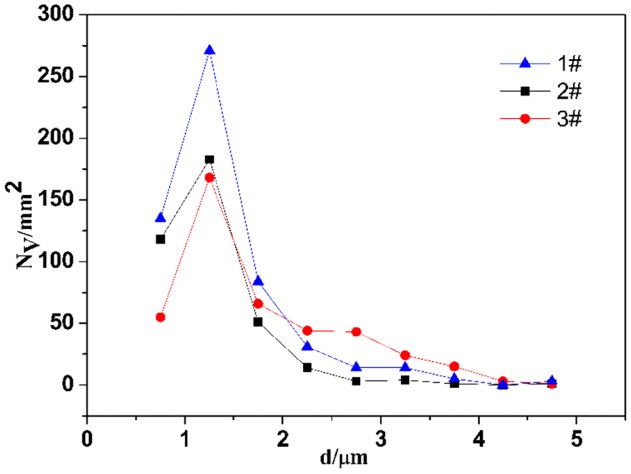

Figure 6: Variation of inclusion density with diameter in test steel.

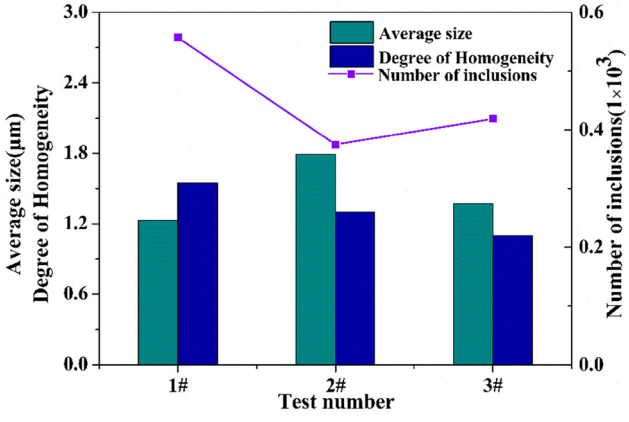

Figure 8: The average size, degree of homogeneity, and number of inclusions in test steel.

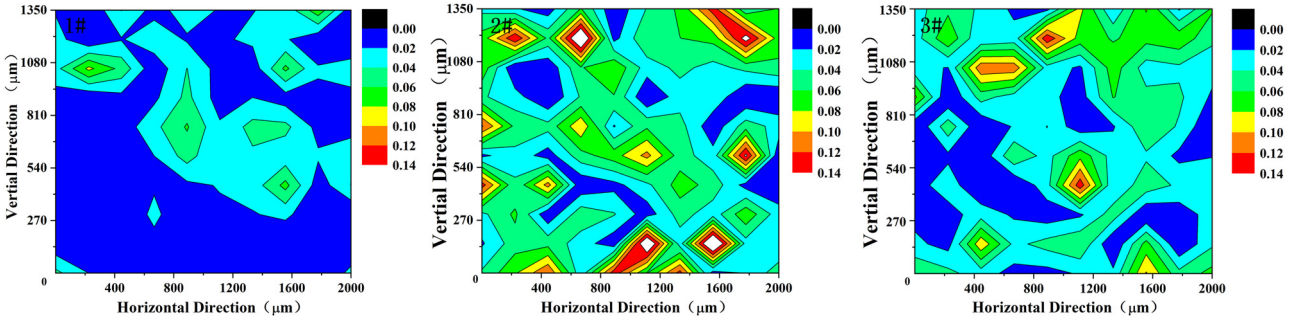

Figure 9: Distribution of area density for inclusions in test steel.

the analysis of the number of inclusions, the number of inclusions in 1# steel is the largest. The results show that the mixed rare earth refined the inclusions in the steel, reduced the size of the inclusions, and increased the number and the degree of homogeneity of the inclusions, which means that the mixed rare earth has a better effect on the modification of the inclusions.

To intuitively describe the distribution of inclusions, the area density distribution map was calculated in Figure 9. Figure 7 is integrated by 100 (10 × 10) SEMs continuously shot (previously proposed in the experimental part), the abscissa represents the *X*-axis direction of the shooting area, the ordinate represents the *Y*-axis direction of the shooting area, and the entire plane represents a summary graph of 100 SEMs. Through the area size of the inclusions in the shooting area, the refinement effect of the inclusions is reflected. The larger the area density of inclusions is (large-scale color accounts for a larger proportion), the more large-size inclusions are and, thus, the worse the refinement effect will be. Figure 7 more intuitively reflects the area distribution of the inclusions, which can be compared with the average size of the inclusions in the previous section to verify the effect of the experiment on the modification of the inclusions again. Comparing the three test steels, the area density of inclusions in 1# steel is concentrated at 0.02, 2# steel is concentrated at 0.08, and 3# steel is concentrated at 0.06. It shows that the area density of inclusions in 1# steel is the smallest, the treatment effect of inclusions is the best, and the distribution of inclusions is the most even. 2# steel has the largest area density and the worst treatment effect. The effect of 3# steel is in the middle. Small-sized inclusions float slowly, and the rare-earth treatment exacerbates the size increase and aggregation of inclusions. As the inclusions accumulate and float, large-size inclusions decrease, the area density of inclusions decreases, and the distribution of inclusions becomes more uniform.

In summary, from the analysis of the morphology, composition, and characteristics of inclusions, the treatment effect of mixed rare earth is better. Through the analysis of the morphology and composition of the inclusions, it is found that the morphology of the inclusions treated by the mixed rare earths is closer to round, and the efficiency of the modification of the inclusions is higher. Through the analysis of the characteristics of the inclusions, the average size of the inclusions treated by the mixed rare earths is smaller and the distribution is more uniform.

4 Thermodynamic calculation

To determine the types of inclusions in molten steel, thermodynamic calculations can be performed on chemical reaction equations. However, it is difficult to determine the type of specific inclusions formed in steel after rare earth is added. The reason is that the oxysulfides in steel are actually complex inclusions, which are very common in steel [25,26]. The type of REM inclusions (oxide/sulfide/oxysulfide) is difficult to determine from the electron microscope image because they also have little change in morphology. Therefore, we can only calculate the chemical reactions related to rare earths in steel and possible rare-earth inclusions through thermodynamic calculations. Table 3 lists the reaction of inclusion transformation and the corresponding standard Gibbs free energy [27–29].

The standard Gibbs free energy of each reaction equation was calculated at a temperature of 1,873 K. The results show that rare earth oxides, rare earth sulfides, rare earth oxysulfides, or complex inclusions may be formed after rare earth is added. Comparing the standard Gibbs free energy, it can be concluded that La and Y have a higher affinity for oxygen than for sulfur. Therefore, the order of inclusions in steel is roughly as follows: rare earth oxides, rare earth oxysulfides, and rare earth sulfides. When the rare earth La and rare earth Y are added, the affinity of La and oxygen and sulfur is higher than that of Y, so the rare earth La reacts first.

Table 3: Standard Gibbs free energy for chemical reaction equations

Reaction	ΔG^θ (J·mol^{-1})
2[Al] + 3[O] = Al_2O_3(s)	−1,225,196 + 393.78 T
2[La] + 3[O] = La_2O_3(s)	−1,511,520 + 379.2 T
[La] + [Al] + 3[O] = $LaAlO_3$ (s)	−1,188,616 + 310.6 T
2[La] + 2[O] + [S] = La_2O_2S(s)	−1,425,820 + 351.0 T
3[La] + 4[S] = La_3S_4(s)	−1,738,380 + 609.6 T
2[La] + 3[S] = La_2S_3(s)	−1,200,990 + 425.0 T
[La] + [S] = LaS(s)	−445,180 + 141.5 T
2[La] + Al_2O_3(s) = La_2O_3(s) + 2[Al]	−286,520 + 270.28 T
2[Y] + 3[O] = Y_2O_3(s)	−1,792,600 + 658.0 T
2[Y] + 2[O] + [S] = Y_2O_2S(s)	−152,100 + 536.0 T
2[Y] + 3[S] = Y_2S_3(s)	−1,171,000 + 441.0 T
[Y] + [S] = YS(s)	−321,080 + 91.0 T
2[Y] + Al_2O_3(s) = Y_2O_3(s) + 2[Al]	−587,482 + 270.28 T

The oxygen activity in molten steel is changing, and the chemical reaction in molten steel is also complicated. Table 4 lists the primary interaction coefficients e_i^j [30–32] of rare earth elements, such as La, Y, O, S, and Al, and other elements in molten steel at 1,873 K.

The mass fraction of each solute element approaches 0, and the solvent ω(Fe) approaches 1. At this time, the secondary interaction coefficienti^j has very little effect on the activity coefficient, and it is taken as 0 in the calculation. According to the chemical composition, the activity coefficient f_i of element i can be calculated by formula (1), and the corresponding activity can be calculated.

$$\lg f_i = \sum_j^n [e_i^j w(j\%) + \gamma_i^j \, wj\%] \, . \tag{1}$$

During the cooling process of molten steel, when the actual solubility product of the precipitate-forming elements is greater than the equilibrium solubility product, a precipitation reaction will occur. In molten steel, the precipitation reaction formula of metal element A and non-metal element B to form $AxBy$ is as follows:

$$xA + yB = A_xB_y, \quad \Delta G = \Delta G^\theta + RT \ln K. \tag{2}$$

When the reaction reaches equilibrium, $\Delta G = 0$. The reaction equilibrium constant K can be expressed as:

$$K = \frac{a_{A_xB_y}}{a_A^x a_B^y} = \frac{1}{f_A^x \cdot w_{(A)}^x \cdot f_B^y \cdot w_{(B)}^y}. \tag{3}$$

Table 4: Interaction coefficient of O, S, La, Y, and Al at 1,873 K (1,600°C)

e_i^j	C	Mn	Si	P	S	Al	O	La	Y
O	−0.45	−0.021	−0.131	0.07	−0.133	−3.9	−0.2	−0.57	−16.3
S	0.11	−0.026	0.063	0.029	−0.028	0.035	−0.27	—	−0.55
La	—	—	—	—	—	—	−4.98	—	−0.006
Y	−0.22	—	—	—	—	—	−90.7	—	–
Al	0.091	—	0.0056	—	0.03	0.045	−6.6	—	—

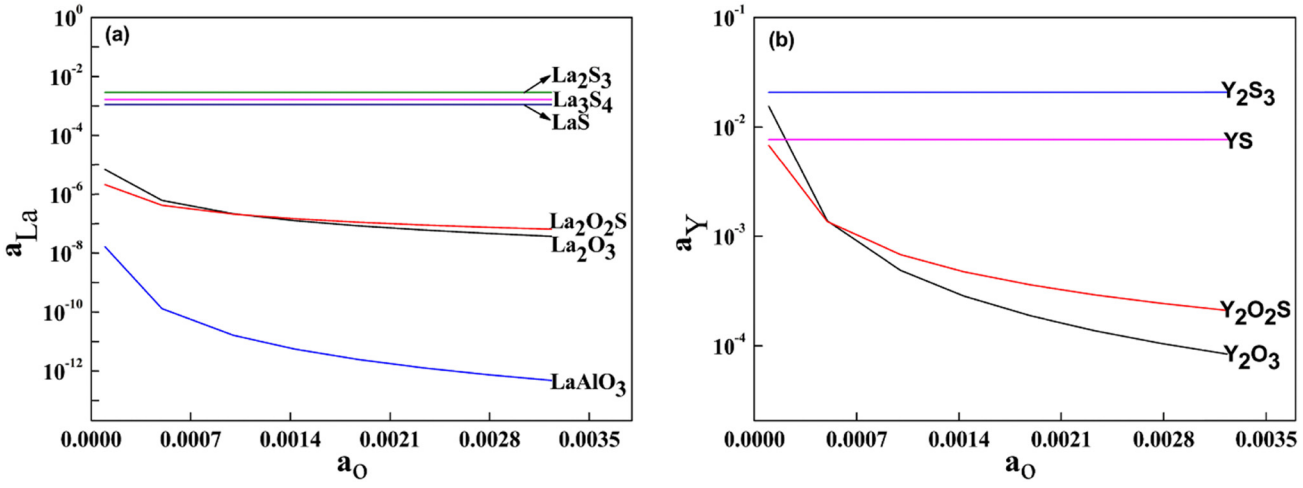

Figure 10: (a) [O] and [La] activity relation graph. (b) [O] and [Y] activity relation graph.

In equilibrium, the temperature is 1,873 K and ΔG is 0. Establish the equilibrium expression of each reaction by formulas (1)–(3) to determine the relationship between the [O] activity and the [REM] activity, and finally get the activity diagram in Figure 10.

Figure 10(a) is a graph of the relationship between the [O] activity and the [La] activity under standard conditions. When the [O] activity is constant, the approximate order of formation of inclusions is as follows: $LaAlO_3 \rightarrow La_2O_3 \rightarrow La_2O_2S \rightarrow LaS \rightarrow La_3S_4 \rightarrow La_2S_3$. When the [O] activity is lower than 0.00108, La_2O_2S inclusions in the steel are formed earlier than La_2O_3 (in practice, the [O] activity is difficult to reach this low). Figure 10(b) is a graph of the relationship between the [O] activity and the [Y] activity under standard conditions. When [O] activity is constant, the approximate order of formation of inclusions is $Y_2O_3 \rightarrow Y_2O_2S \rightarrow YS \rightarrow Y_2S_3$. When the [O] activity is lower than 0.00052, the inclusions Y_2O_2S in the steel are formed earlier than Y_2O_3 (in practice, the [O] activity is difficult to reach such a low level). Through the formation sequence of inclusions, it is concluded that the addition of rare earth will gradually replace Al in Al_2O_3 and finally achieve the modification effect on Al_2O_3 inclusions. We can only roughly understand the reaction of inclusions through thermodynamic calculations. Since the [O] activity and the [REM] activity in molten steel are always fluctuating, it is difficult to accurately grasp the reaction of inclusions. Therefore, the evolution of inclusions can only be roughly determined through thermodynamic calculations and experimental observations (as shown in Figure 11), which is only for readers' reference (in the molten state). La-S in Figure 10 refers to LaS, La_3S_4, and La_2S_3. Y-S refers to YS and Y_2S_3.

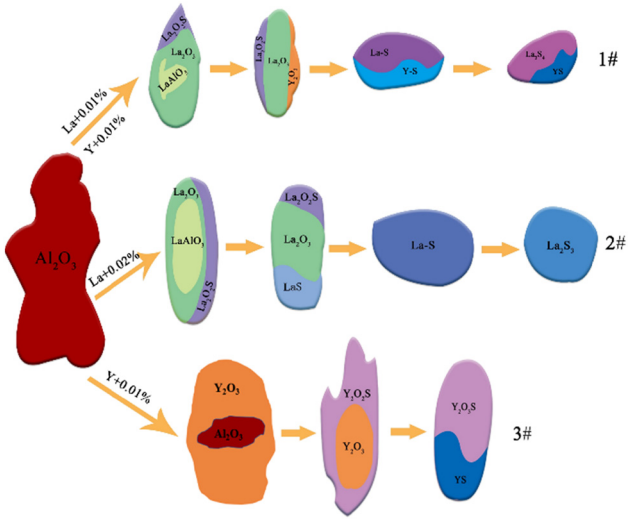

Figure 11: Evolution of inclusions in test steels.

5 Discussion of results

In summary, after adding rare earths, the reactions that occur in steel and the types of inclusions generated are very complicated. Through the analysis of the inclusion composition, we found that the inclusions did react in the steel. The statistical results show that the rare earths have a certain refinement effect on the inclusions in the steel, and the mixed rare earth treatment has the best effect. In addition, comparing the literature data on the size of inclusions in the steel after rare earth treatment [5,10], the average size (1.23 μm) of the inclusions in the steel treated with mixed rare earth is small, indicating that the mixed rare earth has a better refining effect on the inclusions. The better the refinement effect of inclusions is, the higher the performance of steel will be. Rare earth treatment and calcium magnesium treatment have certain modification effects on inclusions. However, few researchers have adopted the mixed rare-earth treatment method; combined with the experimental results of this article, it shows that the mixed rare earth treatment of inclusions in steel has a certain research value.

6 Conclusion

In this article, through related experiments and thermodynamic calculations, the modification effect and modification process of rare earths on inclusions are analyzed. The experimental results and calculation analysis are combined, and the following conclusions are drawn:

1. From the two-dimensional characterization data of the inclusions, it is shown that the addition of rare earths has a refinement effect on the Al_2O_3 inclusions in the test steel.
2. Comparing the size distribution, number density, inter-surface distance, degree of homogeneity, and area density of inclusions in the three test steels, it can be seen that mixed rare earth has the best treatment effect on steel inclusions. The effect of rare earth La treatment is the second, and the effect of rare earth Y treatment is the worst.
3. La and Y have a higher affinity for oxygen than for sulfur. The approximate order of formation of inclusions in steel is as follows: oxides, oxysulfides, and sulfides.

4. In addition to the single rare earth inclusions generated, there are many complex inclusions in the steel.

Acknowledgments: The authors gratefully acknowledge financial support from the National Nature Science Foundation of China (No. 52074095 and NO.51864013).

Funding information: This project is financially supported by the National Science Foundation of China with grant nos. 52074095 and 51864013.

Author contributions: Conceptualization, X.X. and C.L.; methodology, X.X. and C.L.; software, X.X.; writing – original draft preparation, X.X. and L.C.; writing – review and editing, X.X. and C.L.; funding acquisition, C.L. All authors have read and agreed to the published version of the manuscript.

Conflict of interest: The authors declare no conflict of interest.

Data availability statement: All authors can confirm that all data used in this article can be published in the Journal "High Temperature Materials and Processes".

References

[1] Liao, L. L., H. Wei, L. Z. Li, Y. L. Chen, H. F. Yan, and G. H. Liu. Causes and control mechanism of abnormal structure in the center of SWRH82B wire-rod-steel. *Materials Science Forum*, Vol. 944, No. 1, 2019, pp. 294–302.

[2] Luo, S., B. Wang, Z. Wang, D. Jiang, W. Wang, and M. Zhu. Morphology of solidification structure and MnS inclusion in high carbon steel continuously cast bloom. *ISIJ International*, Vol. 57, No. 11, 2017, pp. 2000–2009.

[3] Ferman, M. A., D. N. Rai, J. C. Simmer, and S. F. Kia. Discussion of RE inclusions as heterogeneous nuclei of primary austenitein hardfacing metals of medium-high carbon steels. *Journal of Rare Earths*, Vol. 4, 1999, pp. 293–297.

[4] Hidetoshi, H. Matsuno, and Y. Kikuchi. The Origin of MgO Type Inclusion in High Carbon Steel. *Tetsu to Hagane-journal of the Iron & Steel Institute of Japan*, Vol. 88, No. 1, 2009, pp. 48–50.

[5] Wang, Y., C. Li, L. Wang, X. Xiong, L. Chen, and C. Zhuang. Modification of alumina inclusions in SWRS82B steel by adding rare earth cerium. *Metals - Open Access Metallurgy Journal*, Vol. 10, No. 12, 2020, id. 1696. doi: 10.3390/met10121696.

[6] Zejin, Y. U. Research and analysis of inclusions in SWRH82B steel. *Metal Products*, Vol. 35, No. 2, 2009, pp. 40–42.

[7] Zhao, J., J. C. Bao, S. H. Zhu, Z. Q. Wang, and Z. Yan. Internal defects and reasons of large-size high carbon steel wire rod SWRH82B. *Heat Treatment of Metals*, Vol. 36, No. 4, 2011, pp. 50–54.

[8] Hao, W., L. Jing, S. Chengbin, and Y. Wentao. Transformation of inclusions in H13 steel treated with calcium. *Chinese Journal of Engineering*, Vol. 40, No. s1, 2018, pp. 14–21.

[9] Zheng, W., Z.-H. Wu, G.-G. Li, and C.-Y. Zhu. Effect of Ti-Mg composite deoxidation and sulfur content on the characteristics of inclusions in steel and the precipitation behavior of MnS. *Chinese Journal of Engineering*, Vol. 37, No. 3, 2015, pp. 292–300.

[10] Yue, L., L. Wang, and J. Han. Effects of rare earth on inclusions and corrosion resistance of 10PCuRE weathering steel. *Journal of Rare Earths*, Vol. 28, No. 6, 2010, pp. 952–956.

[11] Huang, Y., G. Cheng, and Y. Xie. Modification mechanism of cerium on the inclusions in drill steel. *Acta Metallurgica Sinica*, Vol. 54, No. 9, 2018, pp. 1253–1261. doi: 10.11900/0412.1961.2018.00079.

[12] Wang, G. Characterization and thermodynamics of Al2O3-MnO-SiO2(-MnS) inclusion formation in carbon steel bill. *Journal of Iron and Steel Research*, Vol. 22, 2015, pp. 566–572.

[13] Xiaofeng, C., B. Yanping, and L. Lu. Evolution and thermodynamic analysis of inclusions during calcium treatment. *Chinese Journal of Engineering*, Vol. s1, 2016, pp. 32–36.

[14] Temuujin, J. and K. Okada. Thermodynamics of modifying effect of rare earth oxide on inclusions in hardfacing metal of medium-high carbon steel. *Chinese Journal of Rare Metals*, Vol. 20, No. 4, 2002, pp. 155–159.

[15] Jiang, Z. H., L. I. Shuang-Jiang, and L. I. Yang. Thermodynamic calculation of inclusion formation in Mg-Al-Si-O system of 430 stainless steel melts. *Journal of Iron and Steel Research*, Vol. 18, No. 2, 2011, pp. 14–17.

[16] Saha, S., T. Ray, S. Basak, and M. Roy. NMR, surface tension and conductivity studies to determine the inclusion mechanism: thermodynamics of host–guest inclusion complexes of natural amino acids in aqueous cyclodextrins. *New Journal of Chemistry*, Vol. 40, No. 1, 2016, pp. 651–661. doi: 10.1039/c5nj02179k.

[17] Guo, J., S. Cheng, Z. Cheng, and L. Xin. Thermodynamics for precipitation of CaS bearing inclusion and their deformation during rolling process for Al-killed Ca-treated steel. *Steel Research International*, Vol. 84, No. 6, 2013, pp. 545–553. doi: 10.1002/srin.201200253.

[18] Kwon, Y., J. Zhang, and H. Lee. Water model and CFD studies of bubble dispersion and inclusions removal in continuous casting mold of steel. *ISIJ International*, Vol. 46, No. 2, 2006, pp. 257–266.

[19] Mu W., H. Shibata, P. Hedström, P. G. Jönsson, and K. Nakajima. *Ferrite formation dynamics and microstructures in inclusion engineered steels with Ti_2O_3 and TiN additions*, Vol. 47, No. 4, 2015, pp. 2133–2147.

[20] Vermeire, M. L., S. Cornu, Z. Fekiacova, M. Detienne, B. Delvaux, and J. T. Cornélis. Rare earth elements dynamics along pedogenesis in a chronosequence of podzolic soils. *Chemical Geology*, Vol. 446, 2016, pp. 163–174.

[21] Rademaker, J. H., R. Kleijn, and Y. Yang. Recycling as a strategy against rare earth element criticality: a systemic evaluation of the potential yield of NdFeB magnet recycling. *Environmental Science & Technology*, Vol. 47, No. 18, 2013, pp. 10129–10136.

[22] Ji, S. I., K. H. Lee, Y. S. Yang, C. Y. Lee, C. M. Bae, and B. M. Kim. The effects of non-metallic inclusion on ductile damage of high

carbon steel wire in multi-pass dry drawing process. *Key Engineering Materials*, Vol. 822, 2014, pp. 155–161.
[23] Li, Y., M. Sun, Z. Jiang, C. Chen, K. Chen, X. Huang, et al. Inclusion modification in C104Cr saw wire steel with different cerium content. *Metals – Open Access Metallurgy Journal*, Vol. 9, No. 1, 2019, id. 54.
[24] Li, Y., L. Wang, C. Chen, J. Li, and X. Li. Effect of Mg treatment on the nucleation and ostwald growth of inclusions in Fe-O-Al-Mg Melt. *Materials*, Vol. 13, No. 15, 2020, id. 3355.
[25] Shin, J. H. and J. H. Park. Formation mechanism of oxide-sulfide complex inclusions in high-sulfur-containing steel melts. *Metallurgical and Materials Transactions B*, Vol. 49, 2018, pp. 311–324.
[26] Krajnc, L., P. Mrvar, and J. Medved. Thermodynamic characterization of multiphase non-metallic inclusions in re-sulphurised steel grades. *Materials and Technologies*, Vol. 48, No. 6, 2014, pp. 923–929.
[27] Tugrul, T. E. Ladle deoxidation, desulphurisation and inclusions in steel -Part 2: Observations in practice. *Archiv Für Dassenhüttenwesen*, Vol. 54, No. 2, 1983, pp. 45–52.
[28] Fruehan, R. J. The free energy of formation of Ce2O2S and the nonstoichiometry of cerium oxides. *Metallurgical Transactions B*, Vol. 10, No. 2, 1979, pp. 143–148.
[29] Wang, H., P. Yu, S. Jiang, B. Bai, L. Sun, and Y. Wang. Evolution of inclusions in steelmaking process of rare earth steels containing arsenic with alumina crucibles. *Metals*, Vol. 10, No. 2, 2020, id. 275.
[30] He, Y., L. Zhang, X. An, G. Wan, W. Zhu, and Y. Luo. Enhanced fluoride removal from water by rare earth (La and Ce) modified alumina: Adsorption isotherms, kinetics, thermodynamics and mechanism. *Science of the Total Environment*, Vol. 688, 2019, pp. 184–198. doi: 10.1016/j.scitotenv.2019.06.175.
[31] Kay, D. A. R., R. K. Dwivedi, and R. V. Kumar. The high temperature thermodynamics of the La-O-S system. *New Frontiers in Rare Earth Science & Applications*, Vol. 10, No. 4, 1985, pp. 1202–1208. doi: 10.1016/B978-0-12-767662-3.50094-2.
[32] Povoden-Karadeniz, E., M. Chen, T. Ivas, A. N. Grundy, and L. J. Gauckler. Thermodynamic modeling of La2O3-SrO-Mn2O3-Cr2O3 for solid oxide fuel cell applications. *Journal of Materials Research*, Vol. 27, No. 15, 2012, pp. 1915–1926.